ChemComm

Accepted Manuscript

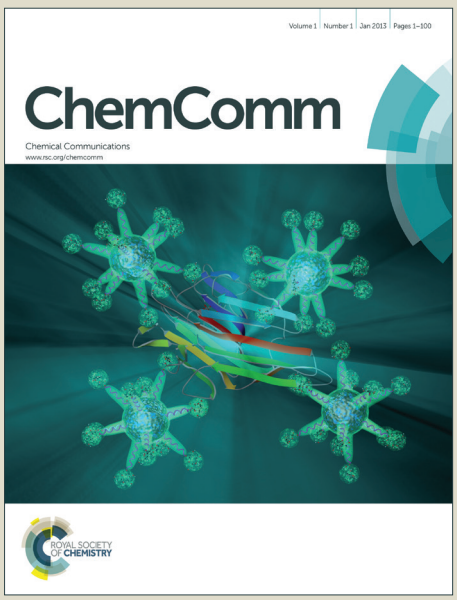

ROYAL SOCIETY OF CHEMISTRY

www.rsc.org/chemcomm

Journal Name

RSCPublishing

COMMUNICATION

Molecular Packing and N-Channel Thin Film Transistors of Chlorinated Cyclobuta[1,2-b:3,4-b']diquinoxalines

Cite this: DOI: 10.1039/x0xx00000x

Received 00th January 2012,
Accepted 00th January 2012

DOI: 10.1039/x0xx00000x

www.rsc.org/

Shuaijun Yang,[a] Danqing Liu,[a] Xiaomin Xu,[a] Qian Miao*[a, b]

Novel chlorinated cyclobuta[1,2-b:3,4-b']diquinoxalines were synthesized and investigated in the solid state. It is found that their molecular packing can be tuned by varying the number and position of chlorine substituents, and 2,8-dichloro-cyclobuta[1,2-b:3,4-b']diquinoxaline either in pure form or as a mixture with its regioisomer functions as n-type semiconductors in organic thin film transistors with field effect mobility of up to 0.42 cm^2/Vs and 0.20 cm^2/Vs, respectively.

Acenes, a family of polycyclic aromatic hydrocarbons (PAHs) consisting of linearly annelated benzene rings as shown in Figure 1a, are one of the most important groups of organic semiconductors, particularly, for organic thin film transistors (OTFTs).[1] With similar linear geometry, linear [*N*]phenylenes (Figure 1a) have benzene rings fused together by four-membered rings, formally with alternating aromatic and antiaromatic characters.[2] Combination of acene and [*N*]phenylene leads to phenylene-containing oligoacenes, which were recently investigated as a new class of fully unsaturated ladder structures.[3] In contrast to acenes, either [*N*]phenylenes or phenylene-containing oligoacenes in the solid state have been rarely explored as electronic materials. Although its structure is closely related to pentacene, a benchmark p-type organic semiconductor for applications in OTFTs, dibenzo[*b*,*h*]biphenylene (Figure 1a) was documented only with two Japanese patents to function as p-type organic semiconductors in OTFTs to the best of our knowledge.[4] Introducing N atoms to acenes leads to N-heteroacenes, which have recently been developed into a class of organic semiconductors with high performance in OTFTs.[5] For example, silylethynylated tetraazapentacene **1a** (Figure 1b)[6] is so far the best semiconductor based on N-heteroacenes with high field effect mobility for electrons.[7, 8] However, the parent compound of **1a**, 5,7,12,14-tetraazapentacene (**1b**), has never been synthesized with unambiguous characterization likely because of its instability. Although Dutt claimed the synthesis of **1b** by condensation of 2,3-diaminophenazine with *o*-benzoquinone,[9] the compound obtained by Dutt was later found to be 5,7,12,14-tetraaza-6,13-pentacenequinone instead.[10] In contrast, cyclobuta[1,2-b:3,4-b']diquinoxaline (**2a**), is a stable molecule combining both motifs of N-heteropentacene and dibenzo[*b*,*h*]biphenylene. Although **2a** was first synthesized four decades ago,[11] the potential application of **2a** and its derivatives for semiconductor materials was not recognized until very recently with a computational study.[12] Here we report new derivatives of **2a** (Figure 1b) with substitution of chlorine atoms, which is an effective design for n-type air-stable organic semiconductors,[13] and demonstrate that the molecular packing of cyclobuta[1,2-b:3,4-b']diquinoxalines can be tuned by varying the number and position of chlorine substituents. It is found that 2,8-dichloro-cyclobuta[1,2-b:3,4-b'] diquinoxaline (**2e**) either in pure form or as a mixture with its regioisomer **2d** functions as n-type organic semiconductors in OTFTs with field effect mobility of up to 0.42 cm^2/Vs and 0.20 cm^2/Vs, respectively, and good air stability.

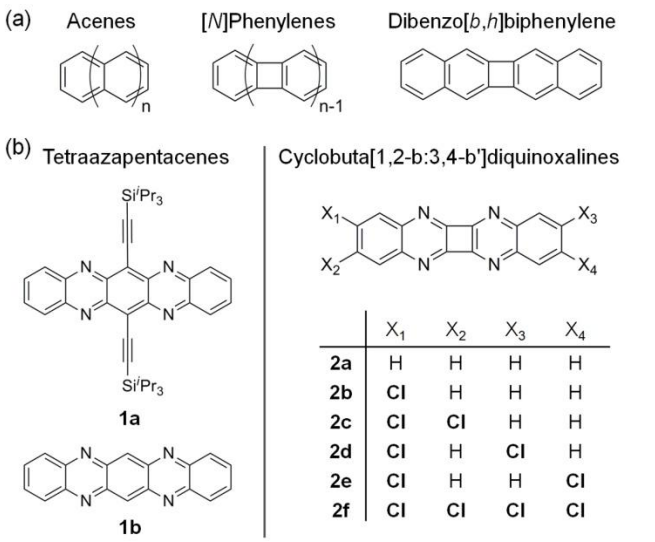

	X_1	X_2	X_3	X_4
2a	H	H	H	H
2b	Cl	H	H	H
2c	Cl	Cl	H	H
2d	Cl	H	Cl	H
2e	Cl	H	H	Cl
2f	Cl	Cl	Cl	Cl

Figure 1 Molecular structures of (a) acenes, [*N*]phenylenes and dibenzo[*b*,*h*]biphenylene; (b) tetraazapentacenes (**1a-b**) and cyclobuta[1,2-b:3,4-b']diquinoxalines (**2a-f**).

As shown in Scheme 1 and detailed in the ESI†, substituted cyclobuta[1,2-b:3,4-b']diquinoxalines **2b-f** were synthesized by modifying the reported synthesis of **2a**.[11] In the synthesis of **2b-e**,

the intermediate **4** was a complicated mixture, which was directly used in the next step without separation. Only in the synthesis of **2f**, the intermediate **4** could be isolated as a pure compound with full characterization. This method yielded dichloro-derivatives **2d** and **2e** as a mixture (**2d**/**e**), which exhibited two sets of peaks in the ^{13}C NMR spectrum (Figure S4 in the ESI†). Chromatography or recrystallization from solutions did not allow separation of the two regioisomers (**2d** and **2e)**. Through a physical vapor transport [14] process, **2e** was isolated in pure form but only in a small amount (Figure S2-4 in the ESI†). Compounds **2a-e** are only slightly soluble (1 mg/ml or lower) in dichloromethane or chloroform, while **2f** is almost insoluble. All compounds **2a-f** are thermally stable in air when heated at 250 ℃ or even higher temperature.

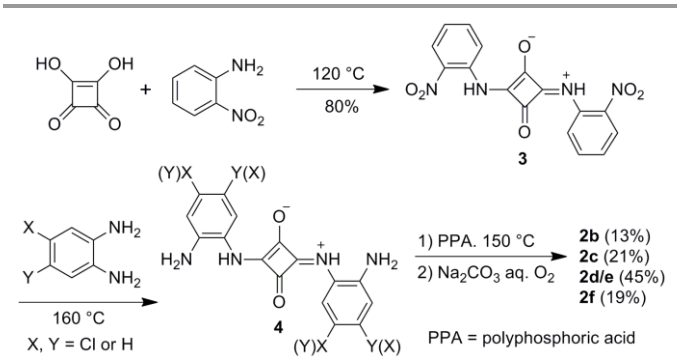

Scheme 1. Synthesis of **2b-f**, where the yield of **2b-f** is indicated as a total yield from **3**.

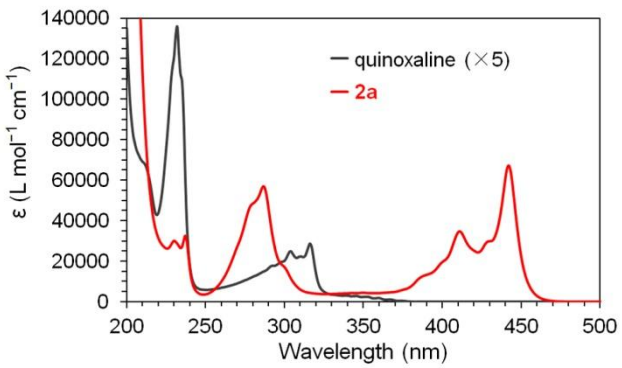

Figure 2. UV-vis spectra for 0.01 mM solutions of **2a** in hexane/CH_2Cl_2 (99:1, v/v) and quinoxaline in hexane.

The energy level of frontier molecular orbitals and the molecular packing of semiconductor molecules are two key factors that determine their performance in OTFTs. To determine the energy levels of highest occupied molecular orbital (HOMO) and lowest unoccupied molecular orbital (LUMO), the cyclobuta[1,2-b:3,4-b']diquinoxalines, except **2d**, which could not be prepared in pure form, were studied with UV-vis absorption spectroscopy and cyclic voltammetry. Yellow solutions of **2a-f** exhibited similar UV-vis absorption with the longest-wavelength absorption maximum at 449 to 471 nm. Figure 2 compares the UV-vis absorption spectrum of **2a** with that of quinoxaline showing that **2a** has a red-shifted and more intense absorption. This suggests considerable conjugation between the two quinoxaline subunits in **2a**, in agreement with the reported absorption spectra of phenylene-containing oligoacenes, which are red shifted relative to the corresponding oligoacenes.[3] Except compound **2f**, all cyclobuta[1,2-b:3,4-b']diquinoxaline exhibited two reduction waves in the test window of cyclic voltammetry (Figure S8 in the ESI†). All of these reduction waves were quasi-reversible with the first half-wave potential in the range of −1.18 V to −0.96 V versus ferrocenium/ferrocene. Based on the reduction potentials [15] and the absorption edges found from the UV-vis absorption spectra, the HOMO and LUMO energy levels of **2a-f** are estimated and summarized in Table 1. It is found that increasing the number of chlorine substituents leads to lower energy levels of both HOMO and LUMO.

Table 1 Absorption edge, reduction potentials and energy levels of frontier molecular orbital for cyclobuta[1,2-b:3,4-b']diquinoxalines.

	Absorption Edge (nm)	E_{red}^1 (V) [a]	E_{red}^2 (V) [a]	HOMO-UMO gap (eV) [b]	LUMO (eV) [c]	HOMO (eV) [d]
2a	465	−1.18	−2.04	2.67	−3.92	−6.59
2b	471	−1.14	−1.91	2.63	−3.96	−6.59
2c	474	−1.08	−1.83	2.62	−4.02	−6.64
2e	475	−1.06	−1.87	2.61	−4.04	−6.65
2f	483	−0.96	—	2.57	−4.14	−6.71

a. Half-wave potential versus ferrocenium/ferrocene. *b.* Estimated from the absorption edge in the UV-vis absorption spectrum from a solution in dicholromethane (1×10^{-5} M) *c*. Estimated from LUMO = −5.10 − E_{red} (eV).[15] *d*. Calculated from the HOMO-LUMO gap and the LUMO energy level.

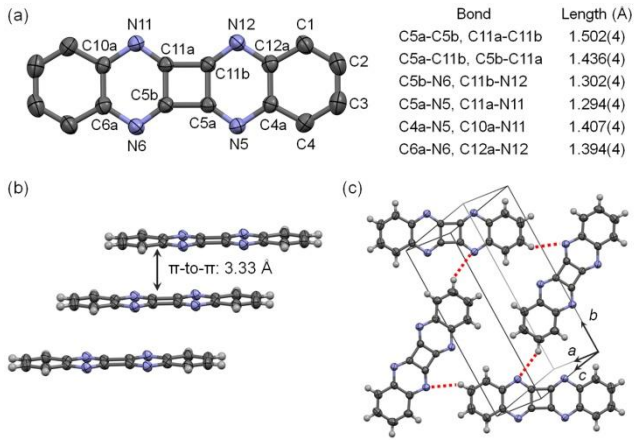

Figure 3 Crystal structure of **2a**: (a) the backbone of **2a** with some C atoms labelled and some bond lengths highlighted (H atoms are removed for clarification); (b) π-π stacking of **2a** ; (c) short contacts (shown as red dashed lines) between molecules of **2a** and the unit cell. (C and N atoms are shown as ellipsoids at 50% probability level.)

Single crystals of **2a** grown from solution in $CHCl_3$ and single crystals of **2b**, **2d/e**, **2e**, **2f** grown by physical vapor transport [14] were qualified for X-ray crystallography. Particularly, when a mixture of **2d** and **2e** was used as the source for physical vapor transport, two types of crystals, namely yellow crystals containing both **2d** and **2e** and orange crystals containing only **2e**, were collected as shown in Figure S2 (the ESI†). The crystal structures of **2a**, **2b**, **2d/e**, **2e** and **2f** show almost the same backbone of dibenzo[*b*,*h*]biphenylene but different motifs of molecular packing.[16] As a representative, the essentially flat backbone of **2a** is shown in Figure 3a. Examination of the bond lengths of **2a** reveals that its central four-membered ring contains four single C-C bonds. Two of them (C5a-C5b and C11a-C11b) are 1.50 Å long, which is even longer than that of the typical nonconjugated single bond between two sp^2-hybridized C atoms (1.47-1.48 Å),[17] and the other two bonds (C5a-C11b and C5b-C11a) are 1.44 Å long, which is longer than typical C-C double bonds in alkenes and arenes but is very close to the conjugated single bond

between two sp^2-hybridized C atoms (1.45-1.46 Å).[17] The four-membered ring is attached to four N atoms with four short C-N bonds (1.29 Å for C5a-N5 and C11a-N11; 1.30 Å for C5b-N6 and C11b-N12), which are not only shorter than other C-N bonds in **2a** but also shorter than the typical bond length of C-N double bonds in imines (1.35 Å).[17] These bond lengths present a radialene-like structure and suggest very poor conjugation between the two quinoxaline subunits. This is however contrary to the considerable conjugation between the two quinoxaline subunits as found from UV-vis absorption spectra.

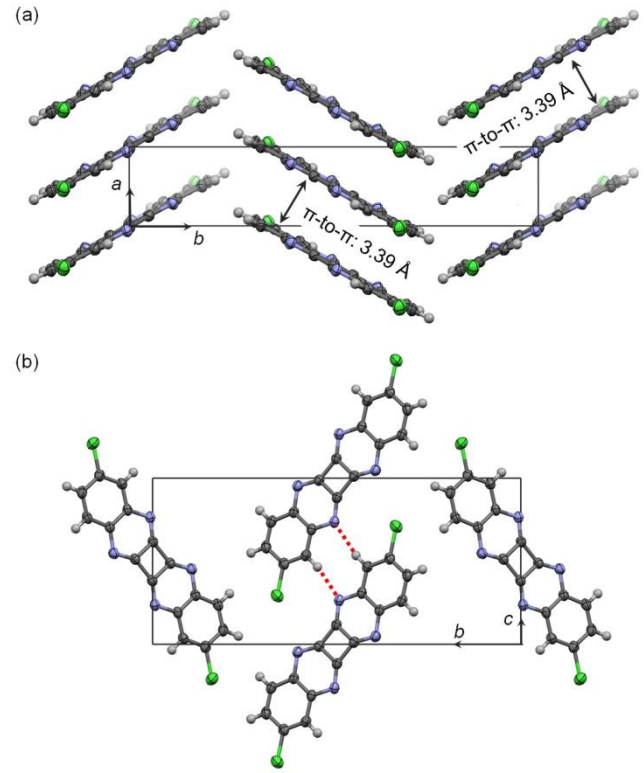

Figure 4 Molecular packing of **2e** (a) as viewed along the *c* axis of the unit cell showing π-π stacking and (b) as viewed along the *a* axis of the unit cell showing weak H-bonds. (C, N and Cl atoms are shown as ellipsoids at 50% probability level.)

As shown in Figure 3b, molecules of **2a** form one-dimensional offset face-to-face π-stacks with a distance of 3.33 Å between two adjacent π-planes. The molecules of **2a** are oriented in two directions, and the π-planes in the two different directions are nearly parallel with a small angle of 4.85 ° between the π-planes. As shown with the red dashed lines in Figure 3c, the neighboring π-stacks of **2a** are linked by C-H ··N weak H-bonds, which involve a H ··N contact (2.65 Å) shorter than the sum of van der Waals radii of H and N atoms and a C-H ··N angle of 146 °. With a disordered arrangement of its Cl atom, **2b** exhibits almost the same crystal structure as **2e**. Figure 4 shows the crystal structure of **2e**, which exhibits one-dimensional offset face-to-face π-stacks similar to those of **2a**. However, unlike those of **2a**, molecules of **2e** are oriented in two directions that intersect with an angle of 53 ° as shown in Figure 4a and form double weak H-bonds between neighboring stacks as shown in Figure 4b. The double H-bonds are associated with a H ··N short contact of 2.57 Å and a C-H ··N angle of 164 °. The molecular packing of **2b** and **2e** differs from that of **2a** likely because the C-H ··N contacts in the crystal structure of **2a** (shown as red dashed lines in Figure 3c) become not available to **2b** and **2e**, which have Cl substituents at the corresponding positions. The co-crystal of **2d/e** contains **2d** and **2e** in a disordered arrangement leading to a molecular packing motif very similar to that of **2f**. Similar to the crystal of **2e**, the co-crystal of **2d/e** exhibits offset face-to-face π-stacks and double weak H-bonds between neighboring stacks as shown in Figure 5. The distance between two adjacent π-planes of **2d/e** is 3.38 Å, and the weak H-bond of C-H ··N contains a H ··N short contact of 2.65 Å and a C-H ··N angle of 168 °. However, unlike **2e**, molecules of **2d/e** are all oriented in the same direction.

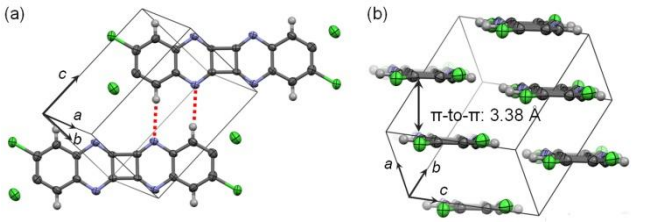

Figure 5 Crystal structure of **2d/e** showing (a) weak H-bonds and (b) π-π stacking. (The green atoms contain disordered Cl and H atoms, non-H atoms are shown as ellipsoids at 50% probability level.)

The low-lying LUMO and π-π stacking of **2a-f** suggest that they can in principle function as n-type semiconductors. To test semiconductor properties of **2a-f** in OTFTs, their thin films were deposited by thermal evaporation under a high vacuum onto a high-*k* dielectric of aluminium oxide and titanium oxide (AlO_y/TiO_x),[18] which was pre-treated with a self-assembled monolayer (SAM) of 12-cyclohexyldodecylphosphonic acid (CDPA shown in Figure 6a). Here, the CDPA-modified AlO_y/TiO_x is a general dielectric as recently developed by us for high-performance vacuum-deposited and solution-processed OTFTs with a capacitance per unit area (C_i) of 210 nF/cm^2.[8] The fabrication of OTFTs was completed by depositing a layer of gold on the organic films through a shadow mask to form top-contact source and drain electrodes. As measured under vacuum, the films of **2e** and **2d/e** functioned as n-type semiconductors with field effect mobility of 0.23 ± 0.07 and 0.11 ± 0.05 cm^2/Vs, respectively. When measured in air, the average mobility of **2e** and **2d/e** decreased to 0.06 ± 0.02 and 0.07 ± 0.03 cm^2/Vs, respectively. Figure 6b shows the transfer I-V curves of the best-performing OTFT of **2e** measured in the saturation regime under vacuum exhibiting field effect mobility of 0.42 cm^2/Vs; and Figure S12 (the ESI†) shows the transfer I-V curves of the best-performing OTFT of **2d/2e** in the saturation regime measured under vacuum and in air exhibiting field effect mobility of 0.20 and 0.16 cm^2/Vs, respectively. In contrast, the thin films of **2a**, **2b**, **2c** and **2f** all appeared insulating in our experiments.

To understand the different performance of **2a-f**, their thin films were investigated with atomic force microscope (AFM) and X-ray diffraction (XRD). The AFM images (Figure S15 in the ESI†) revealed that the films of **2a**, **2b** and **2c** contained isolated crystallites while the films of **2d/e**, **2e** and **2f** were continuous. Particularly, the films of **2e** and **2d/e** exhibited a terraced morphology that is typical for vacuum-deposited film of organic semiconductors. As measured from the section analysis, each terrace step is about 16 Å high (Figure S16 in the ESI†), roughly equal to the length of the long molecular axis in **2d** and **2e** (14 Å). This suggests that molecules of **2e** and **2d/e** stand on the substrate with its long molecular axis roughly perpendicular to the substrate surface. XRD from a 100 nm-thick film of **2a** exhibited two weak peaks at 2θ = 11.7 ° (d spacing = 7.56 Å) and 2θ = 27.7 ° (d spacing = 3.22 Å), which correspond to the (011) and (10−2) crystallographic planes, respectively (Figure S18 in the ESI†), suggesting two orientations of molecules of **2a** on the surface. The diffraction at 2θ = 11.7 °

suggests an edge-on orientation of molecules on the substrate because the (011) plane intersects with the molecular planes at angles of 52.1° and 55.3°, while the diffraction at 2θ = 27.7° suggests a face-on orientation of molecules on the substrate because the (10−2) plane is nearly parallel to the molecular plane as shown in Figure S19 (the ESI†). The film of **2f** exhibited only one X-ray diffraction peak at 2θ = 27.3° (d spacing = 3.26 Å), which corresponds to the (1−12) crystallographic plane. This suggests that molecules of **2f** have a face-on orientation with its π-plane parallel to the substrate surface because the (1−12) plane is nearly parallel to the molecular plane as shown in Figure S19 (the ESI†).[19] In contrast, the films of **2e** and **2d/e** exhibited similar diffraction peaks, which do not correspond to any diffractions as derived from the single crystal structures (Figure S20 in the ESI†), indicating thin film phases that differ from the single crystal phases. The film of **2d/e** exhibited a diffraction at 2θ = 5.54° (d spacing = 15.95 Å) accompanied with three higher-order peaks (corresponding d spacing = 7.95 Å, 5.29 Å, 3.96 Å). These peaks suggest a lamellar structure, and the *d* spacing of 15.95 Å is in agreement with the terrace height found in the AFM image suggesting an edge-on orientation.[19] Therefore the good charge transport in the thin films of **2d/e** and **2e** can be attributed to the edge-on orientation of molecules in a continuous polycrystalline film. In contrast, the absence of field effect in the films of **2a**, **2b**, **2c** and **2f** is likely related to the morphology of isolated crystallites or the face-on orientation, either of which prevents charge transport parallel to the dielectric surface.

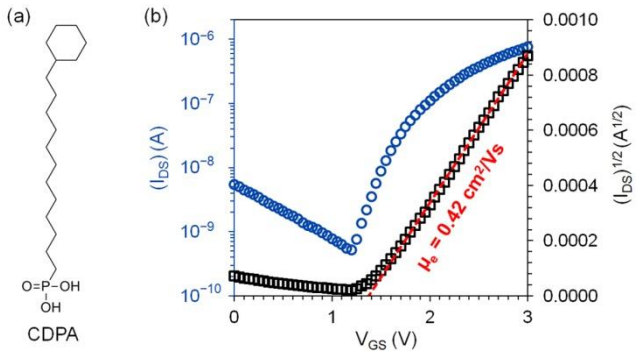

Figure 6. (a) Phosphonic acid that is used to modify the AlO_y/TiO_x dielectric surface in the OTFTs; (b) drain current (I_{DS}) versus gate voltage (V_G) with drain voltage (V_{DS}) at 3 V for OTFT of **2e** with an active channel of W = 1 mm and L = 150 μm as measured under vacuum.

In conclusion, this study puts forth a new design of n-type organic semiconductors by introducing electronegative nitrogen and chlorine atoms into dibenzo[*b*,*h*]biphenylene. A series of new chlorinated derivatives of cyclobuta[1,2-b:3,4-b']diquinoxaline were synthesized and investigated in the solid state. It was found that **2e** and **2d/e** functioned as n-type semiconductors in OTFTs exhibiting field effect mobility of up to 0.42 cm^2/Vs and 0.20 cm^2/Vs and good air stability.

We thank Ms. Hoi Shan Chan (the Chinese University of Hong Kong) for the single crystal crystallography. This work was supported by a grant from the Research Grants Council of Hong Kong (project number: GRF402011) and the University Grants Committee of Hong Kong (project number: AoE/P-03/08).

Notes and references

[a] Department of Chemistry, the Chinese University of Hong Kong, Shatin, New Territories, Hong Kong, China
[b] Institute of Molecular Functional Materials (Areas of Excellence Scheme, University Grants Committee), Hong Kong, China

Electronic Supplementary Information (ESI) available: Synthesis and characterization of **2a-f**, fabrication and characterization of thin film transistors, crystallographic data and crystallographic information files for **2a**, **2b**, **2d/e**, **2e**, **2f** (CCDC 1043927-1043931). For ESI and crystallographic data in CIF or other electronic format, See DOI: 10.1039/c000000x/

1 J. E. Anthony, *Angew. Chem. Int. Ed.*, 2008, **47**, 452–483
2 O. Š. Miljanić, K. P. C. Vollhardt, in *Carbon-Rich Compounds*, (Eds.: M. M. Haley, R. R. Tykwinski), Wiley-VCH, Weinheim, 2006, pp. 140–197
3 R. R. Parkhurst, T. M. Swager, *J. Am. Chem. Soc.*, 2012, **134**, 15351−15356.
4 (a) T. Yamamoto, T. Ohashi, M. Watanabe, *Jpn. Kokai Tokkyo Koho*, JP 2006328006 A 20061207. (b) M. Watanabe, T. Yamamoto, T. Ohashi, *Jpn. Kokai Tokkyo Koho*, JP 2006156980 A 20060615.
5 (a) U. H. F. Bunz, J. U. Engelhart, B. D. Lindner, M. Schaffroth, *Angew. Chem., Int. Ed.*, 2013, **52**, 3810–3821. (b) Q. Miao, *Adv. Mater.*, 2014, **26**, 5541–5549. (c) Q. Miao, *Synlett*, 2012, **23**, 326–336.
6 Z. Liang, Q. Tang, J. Xu, Q. Miao, *Adv. Mater.*, 2011, **23**, 1535−1539
7 D. Liu, X. Xu, Y. Su, Z. He, J. Xu, Q. Miao, *Angew. Chem. Int. Ed.*, 2013, **52**, 6222–6227.
8 D. Liu, Z. He, Y. Su, Y. Diao, S. C. B. Mannsfeld, Z. Bao, J. Xu, Q. Miao, *Adv. Mater.*, 2014, **26**, 7190–7196.
9 S. Dutt, *J. Chem. Soc.*, 1926, **129**, 1171–1184.
10 G. M. Badger, R. Pettit, *J. Chem. Soc.*, 1951, 3211–3215.
11 (a) S. Hünig, H. Pütter, *Angew. Chem. Internat. Edit.*, 1972, **11**, 433. (b) S. Hünig, H. Pütter, *Chem. Ber.*, 1977, **110**, 2532–2544. (c) S. Kanoktanaporn, J. A. H. MacBride, *Tetrahedron Lett.*, 1977, **21**, 1817–1818.
12 M. Schaffroth, R. Gershoni-Poranne, A. Stanger, U. H. F. Bunz, *J. Org. Chem.*, 2014, **79**, 11644–11650.
13 M. L. Tang, J. H. Oh, A. D. Reichardt, Z. Bao, *J. Am. Chem. Soc.*, 2009, **131**, 3733–3740.
14 (a) R. A. Laudise, C. Kloc, P. G. Simpkins, T. Siegrist, *J. Cryst. Growth*, 1998, **187**, 449–454. (b) A. J. C. Buurma, O. D. Jurchescu, I. Shokaryev, J. Baas, A. Meetsma, G. A. de Wijs, R. A. de Groot, T. T. M. Palstra, *J. Phys. Chem. C*, 2007, **111**, 3486–3489.
15 The commonly used formal potential of the redox couple of ferrocenium/ferrocene (Fc^+/Fc) in the Fermi scale is −5.1 eV, which is calculated on the basis of an approximation neglecting solvent effects using a work function of 4.46 eV for the normal hydrogen electrode (NHE) and an electrochemical potential of 0.64 V for (Fc^+/Fc) versus NHE. See: C. M. Cardona, W. Li, A. E.Kaifer, D. Stockdale, G. C. Bazan, *Adv. Mater.*, 2011, **23**, 2367–2371.
16 The crystal structure of **2a** obtained in this study is essentially the same as that reported by R. Allmann, *Cryst. Struct. Commun.*, 1974, **3**, 57.
17 E. V. Anslyn, D. A. Dougherty, *Modern Physical Organic Chemistry*, University Science Books, Sausalito, 2004, chap. 1, p. 22.
18 Y. Su, C. Wang, W. Xie, F. Xie, J. Chen, N. Zhao, J. Xu, *ACS Appl. Mater. Interfaces*, 2011, **3**, 4662–4667.
19 L. Li, W. Hu, H. Fuchs, L. Chi, *Adv. Energy Mater.*, 2011, **1**, 188–193.

Graphical and textual abstracts for the contents pages:

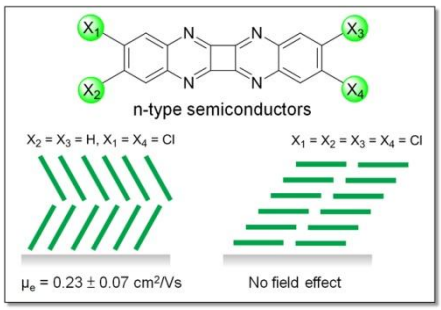

Introduction of chlorine substituents into cyclobuta[1,2-b:3,4-b']diquinoxaline leads to tunable molecular packing motifs and n-type organic semiconductors with field effect mobility of up to 0.42 cm^2/Vs in thin film transistors.